Mantle Transition Zone Thickness in the Central South-American Subduction Zone

Jochen Braunmiller*

Institute of Geophysics, ETH Zurich, Switzerland

Suzan van der Lee

Department of Geological Sciences, Northwestern University, Evanston, Illinois, USA

Lindsey Doermann

Brown University

We used receiver functions to determine lateral variations in mantle transition zone thickness and sharpness of the 410- and 660-km discontinuities in the presence of subducting lithosphere. The mantle beneath the central Andes of South America provides an ideal study site owing to its long-lived subduction history and the availability of broadband seismic data from the dense BANJO/SEDA temporary networks and the permanent station LPAZ. For LPAZ, we analyzed 26 earthquakes between 1993–2003 and stacked the depth-migrated receiver functions. For temporary stations operating for only about one year (1994–1995), station stacks were not robust. We thus stacked receiver functions for close-by stations forming five groups that span the subduction zone from west to east, each containing 12 to 25 events. We found signal significant at the 2σ level for several station groups from *P* to *S* conversions that originate near 520– and 850–900 km depth, but most prominently from the 410- and 660-km discontinuities. For the latter, the *P* to *S* converted signal is clear in stacks for western groups and LPAZ, lack of coherent signal for two eastern groups is possibly due to incoherent stacking and does not necessitate the absence of converted energy. The thickness of the mantle transition zone increases progressively from a near-normal 255 km at the Pacific coast to about 295 km beneath station LPAZ in the Eastern Cordillera. Beneath LPAZ, the 410-km discontinuity appears elevated by nearly 40 km, thus thickening the transition zone. We compared signal amplitudes from receiver function stacks calculated at different low-pass frequencies to study frequency dependence and possibly associated discontinuity sharpness of the *P* to *S* converted signals. We found that both the 410- and 660-km discontinuities exhibit amplitude increase with decreasing frequency. Synthetic receiver function calculations for discontinuity topography mimicking observed topography show that the observed steep topography can adequately explain the observed frequency dependence. The large transition zone thickness beneath LPAZ can be explained by a ~300 K cooler slab or a mantle saturated with water (~1 wt %).

*Now at College of Oceanic and Atmospheric Sciences, Oregon State University, Corvallis, OR.

Earth's Deep Water Cycle
Geophysical Monograph Series 168

10.1029/168GM16

INTRODUCTION

The transition from the upper to the lower mantle in the Earth is bound by two major, globally observed seismic velocity contrasts that occur near 410 km and 660 km depth [e.g., *Dziewonski and Anderson*, 1981]. Mineral physics suggests the discontinuities are due to phase changes from olivine to wadsleyite and from ringwoodite to perovskite and magnesiowüstite at pressures equivalent to these depths [e.g., *Ringwood*, 1975]. The associated increase in S wave velocity for PREM [*Dziewonski and Anderson*, 1981] is 3% and 7%, respectively. Both phase transitions are reported to occur over a fairly narrow (~8 km) depth interval [*Yamazaki and Hirahara*, 1994; *Benz and Vidale*, 1993; *Paulssen*, 1988]. Reasonable temperature variations [*Wood*, 1990] and increasing water content in mantle minerals [*Higo et al.*, 2001] have little seismically detectable effect on the sharpness of the 660-km phase transition. The 410-km phase transition interval, however, might reach widths of up to 20–40 km under hydrous conditions [*Helffrich and Wood*, 1996; *Smyth and Frost*, 2002]. Lower temperatures also widen the interval, but the effect of a cold slab, for example, is much smaller than that of a few tenths of wt % water [*Helffrich and Bina*, 1994; *Helffrich and Wood*, 1996]. Based on observed frequency dependence of P to S converted wave amplitudes, *Van der Meijde et al.* [2003] suggested the 410-km phase transition interval is at least 20 km thick (and in one location 35 km) beneath the Mediterranean region where subduction has been occurring for the past 190 m.y.. Because this thickening is more than plausible from temperatures consistent with tomographically imaged high S velocities [*Helffrich and Bina*, 1994; *Marone et al.*, 2004], the thickening was interpreted as evidence for up to 0.1 wt % of water in the transition zone, brought to depth through subduction.

The overall mantle transition zone thickness also depends on temperature because the 410- and 660-km phase transitions exhibit opposite pressure-temperature Clapeyron slopes [e.g., *Katsura and Ito*, 1989; *Bina and Helffrich*, 1994]. The 410-km transition is exothermic with lower temperatures resulting in decreased pressure (elevated depth) of the phase transition, while the 660-km transition is endothermic and would be depressed under cool conditions. Variations in the depths of the 410- and 660-km discontinuities are thus expected to be anti-correlated near cold subducted slabs resulting in a thickened transition zone. Results from global SS precursor studies [e.g., *Flanagan and Shearer*, 1998; *Gu et al.*, 1998] agree with predicted anti-correlation.

In this study, we calculate receiver functions for stations above the central South American subduction zone to estimate temperature anomalies and water content of the deep upper mantle. To this end we investigate the thickness of the transition zone from the delay time between the P660s and P410s arrivals and the thickness of the olivine to wadsleyite phase transition from analysis of frequency-dependence of receiver functions.

DATA AND METHOD

We are interested in detecting variations of overall mantle transition zone thickness and in characterizing widths of phase transition intervals in well-established subduction zone environments. We thus study the central Andean part of the South American subduction zone because convergence at 50–150 mm/yr is nearly orthogonal since about 50 Ma [*Pardo-Casas and Molnar*, 1987]. In addition, broadband seismic data are available from a dense seismic network. Stations from the temporary BANJO and SEDA networks [*Beck et al.*, 1994], operational from April 1994 to September 1995, and the permanent station LPAZ (Table 1) provide an E-W transect perpendicular and a roughly N-S oriented transect parallel to the strike of the subduction zone (Figure 1). Seismicity defines the subducting slab down to ~350 km depth and between 490 to 640 km depth (Figure 1); slab continuity through the aseismic zone is indicated by seismic tomography [*Bijwaard et al.*, 1998].

We calculated receiver functions from teleseismic earthquakes in the 30°–95° distance range with magnitude M ≥ 6.0 (Figure 2). Most events producing quality receiver functions (Table 2) occurred in the Central American and Mexican subduction zones with back-azimuth 310°–325° and some in the South Sandwich Islands region with back-azimuth 145°–180°. Receiver functions were obtained through frequency domain deconvolution [*Langston, 1979*; *Ammon, 1991*]. We deconvolved 90 s long vertical from 250 s long radial (and transverse) component data, each window starting 20 s before the P wave arrival. We filled spectral gaps to stabilize the deconvolution such that amplitudes on the vertical component were at least 10% of its peak value (0.1 water level). Seismograms were high-pass filtered at 0.05 Hz prior to deconvolution and receiver functions were computed for nine low-pass corner frequencies between approximately 0.15 and 0.75 Hz. We inspected seismograms and radial and transverse receiver functions visually to select quality receiver functions for depth conversion and later stacking. We used the *iasp91* velocity model [*Kennett and Engdahl*, 1991] to perform a pre-stack time-to-depth conversion. Resulting absolute depths are thus probably biased, given that we ignore lateral heterogeneity associated with subduction zones. Our main interest is to determine the transition zone thickness, and since this derives from relative rather than absolute timing of two converted phases it is virtually insensitive to lateral heterogeneity in the top 400 km. Our

Table 1. Station list. #: Station number. EU: number of events used; about 50% of all events could be used. Thickness, 410, 660: transition zone thickness, nominal depth of 410- and 660-km discontinuity with 1σ uncertainty from averaging over 9 frequencies for each station group (Figure 3); 'central-east' group values are from amplitudes not significant at 2σ-level. 410F and 660F indicates probability for frequency dependence of amplitudes based on Gaussian distribution test. Stations 1–3, 4–6, 7–11, 13–17, and 18–20 are 'west', 'central', 'north', 'central-east', and 'far-east' station groups.

#	Name	Latitude [°]	Longitude [°]	EU	Thickness [km]	410 [km]	660 [km]	410F [%]	660F [%]
1	PICH	-19.869	-69.420	3					
2	LIRI	-19.852	-68.849	3	254±1	417±1	671±2	79	24
3	HIZO	-19.607	-68.326	6					
4	SALI	-19.621	-67.726	9					
5	DOOR	-19.354	-67.223	9	274±3	430±2	704±1	84	75
6	CHIT	-20.077	-66.886	5					
7	POOP	-18.387	-67.018	4					
8	CHUQ	-17.945	-67.818	5					
9	LAJO	-17.776	-67.479	3	276±1	425±3	700±2	91	71
10	SICA	-17.292	-67.749	5					
11	COLL	-16.922	-68.314	2					
12	LPAZ	-16.173	-68.078	26	296±6	369±1	666±5	81	67
13	TACA	-18.828	-66.734	7					
14	CRUZ	-19.103	-66.221	6					
15	CRIS	-19.375	-65.932	2	(290)	(400)	(690)		
16	BATO	-19.626	-65.437	4					
17	YUNZ	-19.158	-65.069	6					
18	SCHO	-19.148	-64.643	9					
19	ROSL	-19.486	-64.178	8					
20	PICH	-19.811	-63.721	3					

procedures follow *Van der Meijde et al.* [2003] such that inferences based on depth-converted receiver functions can be directly compared with their interpretations.

RESULTS

The pre-stack depth-converted receiver function stacks are shown for each station group in Figure 3 for the nine investigated low-pass filters (0.75 to 0.15 Hz from left to right); the shaded area corresponds to amplitudes larger than zero at the 95% confidence level (mean minus 2 standard deviations). Station groups and number of events analyzed are given in Table 1. Table 1 also lists results for transition zone thickness and nominal depths of the 410- and 660-km discontinuity derived for the *iasp91* velocity model.

For permanent station LPAZ, we obtained 26 quality receiver functions (Table 2) from 62 analyzed events from 1993 to 2003. The receiver function stack reveals significant signals from the upper mantle phase transitions.

For the 19 BANJO/SEDA stations, we could analyze maximally 17 events (SCHO) per station due to the relatively short-term deployment resulting between only 2 (CRIS and COLL) and 9 (DOOR, SALI, and SCHO) quality receiver functions. Individual station stacks usually did not yield stable results and we grouped stations located at similar positions relative to the subducting slab (Figure 1). These multi-station stacks (Figure 3) show signals from mantle converted phases. We tested signal robustness by repeating the stacking process for the 'west' group, which has fewest events (12), each time omitting one different receiver function. The resulting 12 stacks composed of the 11 remaining receiver functions showed no significant differences and we conclude that our stacks are stable and indeed reflect subsurface structure.

For the LPAZ and 'central-east'-group stacks, containing the largest number of events (26 and 25, respectively) we investigated the effect of event back-azimuth by stacking only events from northwest and south, respectively. The northwest sub-stacks, which contain most events, are stable and more closely resemble the overall stacks than south sub-stacks. Differences between the sub-stacks are presumably due to rays sampling different mantle parts above, below or inside the slab. The differences also result in incoherent stacking, with incoherency decreasing with decreasing signal frequency.

Observed Phase Transitions and Mantle Transition Zone Thickness

The 'west' stack is composed of three stations located ocean-ward where the slab is above the mantle transition zone

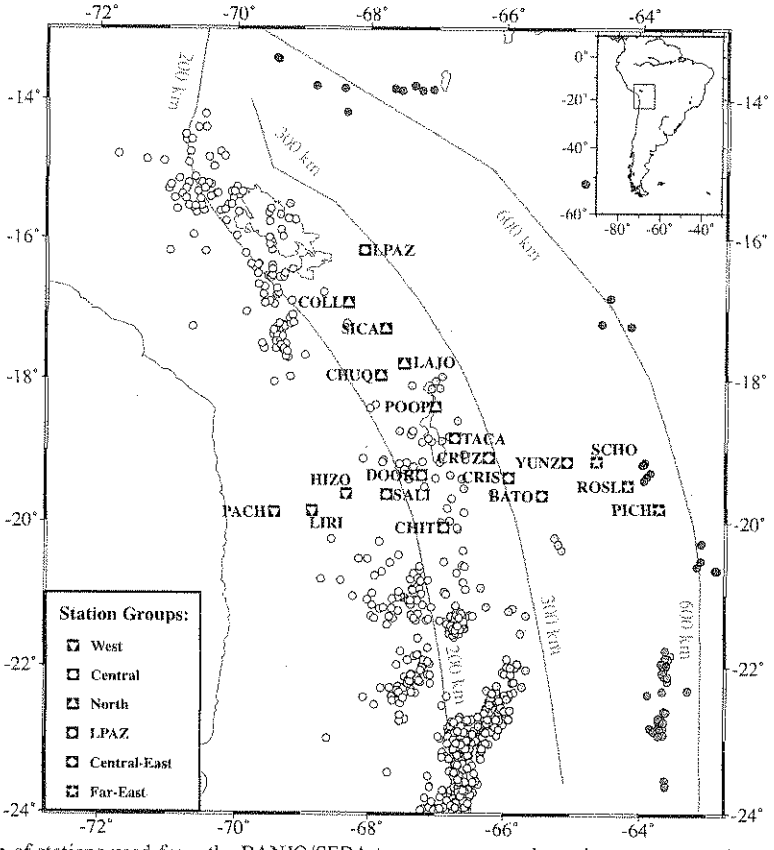

Figure 1. Map of stations used from the BANJO/SEDA temporary networks and permanent station LPAZ. Legend (lower left) indicates station groups for receiver function stacks. Earthquake epicenters are from the Engdahl et al. [1998] catalog with darker gray shading according to four depth intervals (150–250, 250–350, 450–550, and 550+ km depth, no events occurred between 350 and 490 km depth). 200-, 300-, and 600-km Wadati-Benioff zone contours are from Hasegawa and Sacks [1981] and Cahill and Isacks [1992]. Inset (upper right) shows study area.

(Figure 1, Table 1) and we expect to find undisturbed 410- and 660-km discontinuities. The stack shows clear conversions near 417 km and 671 km depth (Figure 3). We also detect conversions near 740 km and 870 km depth (and possibly a weak signal from ~500 km depth). These depths (and others cited in Table 1) are averages determined at maximum amplitudes for 2σ-significant signals at nine frequency bands; uncertainties are simply one standard deviation from averaging and do not include picking errors or systematic errors due to differences between real velocity and *iasp91*. Absolute depths could be overestimated because *iasp91* has a thinner crust than the Andes, which includes a 40–70 km thick slow felsic crust [*Beck and Zandt*, 2002], but could be underestimated because *iasp91* has lower velocities than the seismic velocities in cold subducting lithosphere. Accounting for differences in the upper 70 km alone could systematically raise all conversion depths by roughly 5–15 km (larger values for thick crust). However, the transition zone thickness of 254 km (Table 1) is normal compared to the 250 km of 1D Earth model *iasp91* and slightly thickened compared to a global average of about 242 km [*Flanagan and Shearer*, 1998]; our absolute thickness uncertainties are probably less than ±10 km.

The 'central' and 'north' groups are located at similar positions relative to the down-going slab (Figure 1). Both groups show clear conversions from the 410- and 660-km discontinuities at nominal depths near 425–430 km and 700–705 km. The transition zone thus thickens from west to east to 274 km and 276 km, respectively. Additional conversions are detected from about 530–535 km and from 845 and 875 km depth, respectively.

The LPAZ stack shows a conversion near 369 km depth indicating a significant 40-km elevation of the 410-km phase

transition. *Collier and Helffrich* [2001, their Fig. 6) also found a similarly elevated phase transition depth near the LPAZ 410-km conversion points (Figure 4). Conversions for northwestern events, which dominate the stack, occur where the slab top is ~300 km deep and the slab dips steeply (Figure 4). The 410-km conversion thus probably occurs inside the cold slab and is elevated. We found a fairly normal value of 666 km depth for the 660-km phase transition, which may or may not be biased because of ignored lateral heterogeneity. Overall, the transition zone thickness is widened to about 296 km. We also found signal originating near 915 km depth; but found no clear signal from near 500 km depth.

The 'central-east' and 'far-east' stacks are composed of stations where the Benioff zone beneath dips steeply and its top is between 300 and 600 km depth. Both groups show no clear signal from the 410- or the 660-km discontinuity. Weak signals, not significant at 2σ, possibly indicate a transition zone thickness of ~290 km for the 'central-east' stack. For the 'central-east' stack, we found significant signal amplitudes only at 500 km and 860 km depth. The group's stations are located at a similar position relative to the down-going slab as LPAZ, which shows both phase conversions. We attribute the absence of coherent signal for the 'central-east' group to possible differences in sampling relative to the slab. At LPAZ, signal stacks coherently because most conversion points occur at similar slab depth and thus similar discontinuity depth (Figure 4). This is likewise further west (Figure 4) where the slab is above the 410-km discontinuity and dips relatively gently ('western' and 'central' groups) or, for steeper dip, conversions occur at similar position (depth) relative to the slab ('north' group). In contrast, conversions for eastern groups occur at different positions relative to the steeply dipping slab thus sampling the discontinuities at varying depths such that signal stacks incoherently. This effect is strongest for the 'far-east' group where we found no significant signal from any depth across the frequencies investigated. For the eastern groups, stacking all events thus does not enhance the signal; we suspect stacking events from small source regions would provide coherent signal for specific small conversion regions. However, data quantity is insufficient to obtain reliable stacks from subsets of events for each eastern station group.

Frequency Dependence of Phase Transition Intervals

We calculated receiver function stacks for nine different frequency bands (Figure 3). Amplitudes (and widths) of the 410- and 660-km phase transition signals clearly change with frequency. The amplitudes in Figure 3 are relative to the direct P wave, set to 1, and reach a maximum of 0.133 for the lowest frequency (0.15 Hz) of the 'west'-groups' 410-km

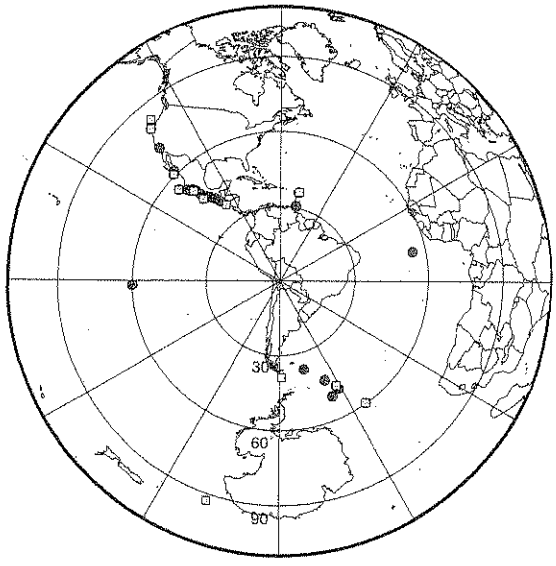

Figure 2. Teleseismic earthquakes used for analysis in equidistant azimuthal projection (thin lines are 30°-distance steps). Dark circles are events used for LPAZ; light squares for BANJO/SEDA stations. Most events are located in Central and North America northwest of the study area, dominating our receiver function stacks.

signal. We observe three trends. First, amplitudes generally increase form high to low frequencies (from left to right) for each phase in each stack. Second, amplitudes vary by a factor of about 2 for the 410-km signal, but only by about 1.5 for the 660-km signal. This is consistent with a wider transition interval for the 410- than for the 660-km phase transition. Signal near 520-km depth, visible for the 'north', 'central', and 'central-east' stacks, is marginal at high frequencies (0.75 Hz) particularly for the otherwise normal 'north' and 'central' stacks, indicating an even wider transition interval for the wadsleyite to ringwoodite phase transition. And third, low frequency amplitudes are larger for the 410- than for the 660-km transition indicating that the shallower phase transition has a stronger impedance contrast, which is in contrast to global velocity models (e.g. *iasp91*).

Following *Van der Meijde et al.* [2003], we estimated frequency dependence of signals from the 410- and the 660-km discontinuity by comparing Gaussian distributions given by the stacks' mean amplitude and standard deviation for highest and lowest frequency receiver function. The non-overlapping area of the two Gaussians then represents the probability of frequency dependence. We read mean amplitudes and standard deviations from the stacks for each group where both phases were present and calculated the probability of frequency dependence (Table 1).

Table 2. Events used for receiver function analysis. Locations and depths are from the PDE catalog, Mw from Harvard CMT, b: body wave magnitude.

Date	Latitude [°]	Longitude [°]	Depth [km]	Magnitude M_w	Station Used
1993/09/10	14.72	-92.65	34	7.3	12
1993/09/27	-53.65	-51.62	33	6.6	12
1993/09/30	15.42	-94.70	19	6.5	12
1993/10/24	16.76	-98.72	21	6.6	12
1994/01/17	34.21	-118.54	18	6.7	12
1994/02/12	-10.79	-128.80	15	6.7	12
1994/05/23	18.17	-100.53	55	6.3	12
1994/07/04	14.89	-97.32	15	6.5	3–15, 17–20
1994/07/25	-56.36	-27.37	81	6.3[b]	3–11,13,17–20
1994/09/01	40.40	-125.68	10	7.0	3–4,6–8,10,13–14,17–19
1994/10/27	43.52	-127.43	20	6.3	5
1994/12/10	18.14	-101.38	48	6.4	1–2,4–10,13,17,19
1995/01/03	-57.70	-65.88	14	5.9	4–6,15,17–19
1995/02/19	40.56	-125.54	10	6.6	8,10,12–13,18–19
1995/03/08	16.56	-59.56	8	6.2	12–13,16–20
1995/05/23	-55.95	-3.36	10	6.8	4–5,12,14,18
1995/05/31	18.96	-107.42	33	6.3	1–5,13–14,18–19
1995/06/14	12.13	-88.36	25	6.6	3–5,8,16
1995/06/21	-61.67	154.77	10	6.7	16
1995/06/30	24.69	-110.23	10	6.2	1–5,12,14,16,18
1995/08/28	26.09	-110.28	12	6.6	12
1995/09/14	16.78	-98.60	23	7.4	12
1996/01/22	-60.61	-25.90	10	6.2	12
1996/02/18	-1.27	-14.27	10	6.6	12
1997/01/11	18.22	-102.76	33	7.2	12
1997/04/22	11.11	-60.89	5	6.7	12
1997/05/01	18.99	-107.35	33	6.9	12
1997/05/22	18.68	-101.60	70	6.5	12
1998/02/03	15.88	-96.30	33	6.4	12
2002/11/12	-56.55	-27.54	120	6.2	12
2002/11/15	-56.05	-36.40	10	6.7	12
2002/12/18	-57.09	-24.98	10	6.1	12
2003/01/21	13.63	-90.77	24	6.5	12
2003/01/22	18.77	-104.10	24	7.5	12

The statistical test confirms our visual observation that signal amplitude for both discontinuities increases with decreasing frequency. Probabilities are generally higher for the 410-km (all >75%) than for the 660-km discontinuity (all ≤75%) and, except for the 660-km discontinuity of the 'west' group, are always significant (>66%). A conventional two-sample t-test confirmed the high statistical likelihood for frequency dependence. Part of the frequency dependence may be the result of data processing as we also found some (30 %) frequency dependence in P410s from stacks of synthetic receiver functions for a flat discontinuity. The apparent frequency dependence in synthetics for a flat interface is due to negligible standard deviations of P410s amplitudes, making small variations in amplitude seem significant; for observed data, the standard deviations are not negligible.

DISCUSSION

Frequency dependence of the P to S converted signal amplitude had been found earlier for some stations in the Mediterranean region [*Van der Meijde et al.*, 2003]. There, only the 410-km signal showed strong dependence while the 660-km signal varied little with frequency. *Van der Meijde et al.* [2003] interpreted their observations as indicating a sharp 660-km phase transition and a thickened 410-km phase transition interval, implying the presence of as much as 500–1000 ppm by weight of water in olivine. They suggested

the water is brought into the mantle by subduction processes from above. Here we have studied P to S converted signals from mantle discontinuities in the long-lived, stable South American subduction zone to test their inferences.

We found strong frequency dependence for the 410-km, but contrary to *Van der Meijde et al.* [2003] also significant dependence for the 660-km discontinuity. Our results could imply that both phase transitions occur over a wider than usual depth interval; however, significant widening of the 660-km transition due to temperature variations or increased water content is not expected [*Wood*, 1990; *Higo et al.*, 2001]. Furthermore, we stack spatially distributed converted signals for station groups in a steep-relief environment while *Van der Meijde et al.* [2003] stacked spatially concentrated converted signals for single stations atop gentler discontinuity topography, which yields the present study more susceptible to incoherent stacking. Discontinuity relief not only affects timing of the converted phases in seismograms but also scatters their energy, distorting the waveforms. An interpretation in terms of scattering by discontinuity relief is consistent with stacks from LPAZ and the 'central-east' group. Conversions for LPAZ are closely spaced resulting in coherent stacks; conversion points of the group are widely distributed (Figure 4), sample the slab at different depths

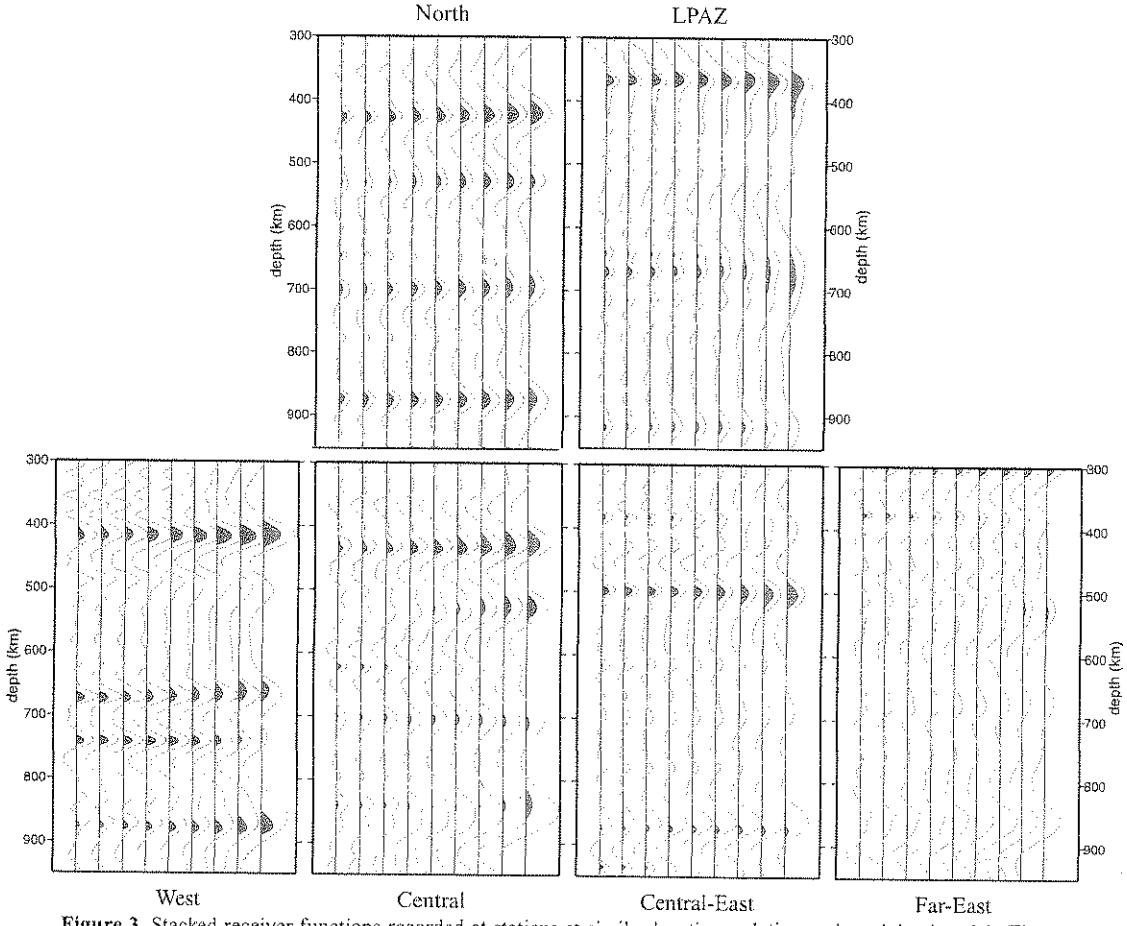

Figure 3. Stacked receiver functions recorded at stations at similar locations relative to the subducting slab (Figure 1 and Table 1). Each panel shows receiver function stacks for nine different low-pass filters with corner frequencies (from left to right) at 0.75, 0.63, 0.5, 0.4, 0.35, 0.3, 0.25, 0.2, and 0.15 Hz, respectively. Solid lines are average values; shaded areas indicate signal is greater than zero at 95% confidence level (2σ). Absolute depths, based on *iasp91* velocity model, ignore velocity heterogeneity and could thus be biased; depth difference estimates (mantle transition zone thickness), however, are robust.

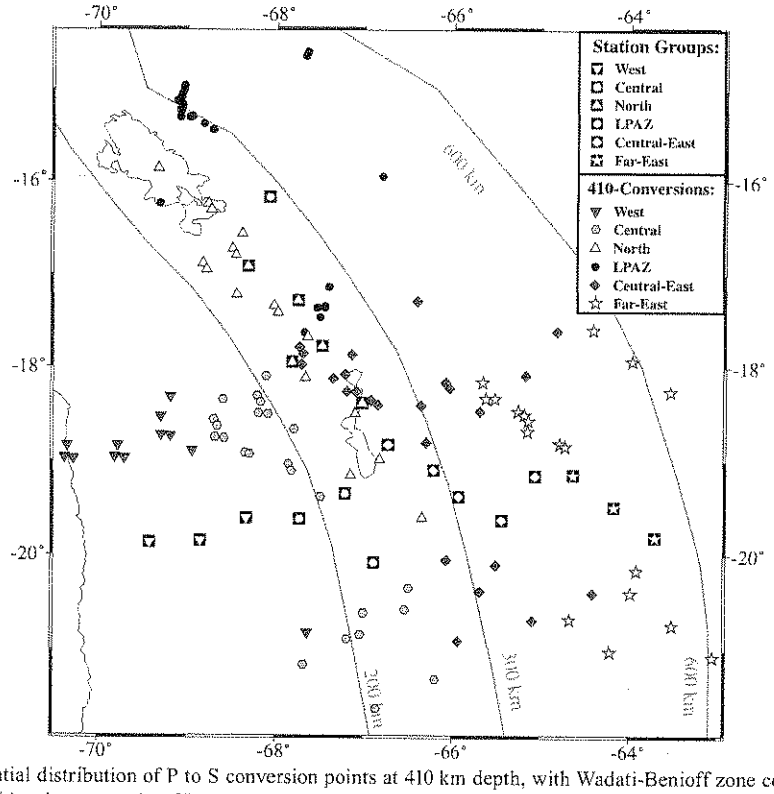

Figure 4. Spatial distribution of P to S conversion points at 410 km depth, with Wadati-Benioff zone contours. Note that groups with coherent stacks of P410s have conversion points predominantly under the slab (west, central) or in the slab and roughly parallel to the slab-depth contours (north, LPAZ), whereas eastern group conversions, resulting in incoherent stacks, occur near or above a steeply dipping slab. Position of conversion points are approximate and do not account for lateral heterogeneity.

and signal stacks incoherently. Multiple-station stacks are coherent further west where phase transitions occur below the slab and the slab has no or only slight influence on the transition depths.

A thickened transition zone can be explained by lowered temperatures or by elevated water content. The observed thickening of the transition zone from 255 km below the slab to 295 km where the slab enters the transition zone (Figure 3) over a lateral distance of about 200 km implies a steep relief on one of or both the 410- and 660-km discontinuities with a maximum amplitude of ~40 km. Absolute depths, although not as well constrained, imply almost all of this relief is on the 410-km discontinuity. However, the P660s signal is less coherent at higher than at lower frequencies suggesting the 660-km discontinuity also has relief.

Most 410-km Ps conversion points for LPAZ (Figure 4) occurred within the slab. Assuming the 660-km discontinuity beneath LPAZ is truly at 666 km depth (Table 1) requires a 34-km uplift of the 410-km discontinuity. This uplift implies the slab would be about 250–350 K cooler, using a range of Clapeyron slopes [*Bina and Helffrich*, 1994; *Katsura et al.*, 2004], than the surrounding mantle. If this thermal anomaly extends to the 660-km discontinuity, its small (6 km) associated depression would be consistent with the gentle Clapeyron slopes recently inferred for the ringwoodite to perovskite and ferropericlase transition [*Litasov et al.*, this volume], but inconsistent with relief causing the frequency-dependence of P660s. Using the Clapeyron slopes of *Bina and Helffrich* [1994] of 9 km uplift and 6 km depression per 100 K cooling for the 410-km and 660-km discontinuity, respectively, we obtain a vertically homogeneous temperature anomaly of -267 K, ascribing 24 km to uplift of the 410-km discontinuity and 16 km of downwarp to the 660-km discontinuity. However, the transition-zone can also thicken in the presence of water because of the great water storage capacity of transition zone minerals [*Smyth and Jacobsen*, this volume; *Higo et al.*, 2001; *Wood*,

1995; *Smyth and Frost*, 2002; *Hirschmann et al.*, this volume]. If the slab or nearby mantle is hydrous (up to a few tenths of wt % water), it could explain up to about 20 km [*Smyth and Frost*, 2002; *Hirschmann et al.*, this volume] of the uplifted 410-km signal, leaving the slab only 50–150 K cooler. However, such hydration would also thicken the 410-km discontinuity itself by about 20 km and cause a stronger frequency dependence of converted signal from the discontinuity unless the mantle was entirely saturated with water [*Chen et al.*, 2002; *Hirschmann et al.*, this volume]. In the latter case the discontinuity would be sharp and produce frequency-independent seismic conversions, but could have a thin layer of melt atop (*Karato et al.*, this volume; *Hirschmann et al.*, this volume].

We also examined whether such extreme discontinuity relief (a 15° slope] affects frequency dependence by calculating synthetic receiver function stacks for a discontinuity with relief [following *Van der Lee et al.*, 1994]. The relief is a steep Gaussian-shaped hill or dip in the direction perpendicular to the strike of the slab and is constant parallel to it. The Gaussian hill or dip has a half width of 60 km and amplitude of 50 km. We used the same event-station geometry and processing steps in these calculations as for the data. A 50-km up-warp, simulating an elevated 410-km discontinuity within the slab, results in a high (70%) probability for frequency dependence while a 50-km down-warp, mimicking a depressed 660-km discontinuity, has a 50% probability. Frequency dependence is caused by signal focusing and scattering because of the curved interfaces. Our tests show that steep relief can explain most of the observed frequency dependence. However, we performed the tests for the eastern station groups; to reconcile the discrepancy between clear synthetics and lack of observed signal probably implies that the actual relief or shape of the discontinuity is more complicated than in our model, or that discontinuity thickening plays a more important role east of the slab. 3-D velocity heterogeneity would cause further differences in Ps arrival time, even for a flat discontinuity, and contribute to incoherent stacking.

In addition to signals from the 410- and 660-km discontinuities, we found significant amplitudes near 520-km depth for the 'north', 'central' and 'central-east' groups. The exothermic wadsleyite to ringwoodite phase transition occurs around this depth, but the transition interval is broad [e.g., *Helffrich*, 2000] and a 520-km discontinuity is mainly seen using long-period seismic data [*Shearer*, 1990]. This is consistent with our stacks that show increased significance for signal amplitudes with lower frequencies. We also observe coherent signals from a depth of around 850–900 km with signal strength apparently decreasing from west to east (where the signal is absent). Discontinuities in the upper part of the lower mantle with limited spatial extent have been reported in the literature [e.g., *Kawakatsu and Niu*, 1994], but their origins are currently unknown.

CONCLUSIONS

We conclude that subduction of the Nazca plate is associated with extreme transition-zone thickening over short lateral distances. Such thickening can be caused by cooler temperatures, increased water content in the transition zone, or both. The observed frequency dependence of P to S signals generated at the 410- and 660-km phase transitions in the South American subduction zone is probably predominantly due to this steep discontinuity relief rather than thickened phase transition intervals. Normal transition intervals occur in a water-saturated mantle as well as in a dry mantle. In the absence of water, our results imply a slab up to 350 K cooler than the mantle trenchwards. The presence of close to 1 wt % of water (up to saturation) in or near the slab can explain some of the transition-zone thickening but not all, leaving an inferred temperature anomaly of 150 K at most. Our study documents characteristics of the transition zone in a subduction environment, most notably extreme thickening of the transition zone where the slab is thought to penetrate it. However, our data provide insufficient resolution, particularly because of the limited duration of seismic experiments, to establish the presence or absence of water.

Acknowledgements. BANJO/SEDA and LPAZ seismic data were obtained from the Incorporated Research Institutions for Seismology (IRIS) Data Management Center. This study is based upon work performed by LD during an IRIS Summer Undergraduate Internship at the ETH Zurich, Switzerland supported by IRIS under their Cooperative Agreement No. EAR-0004370 with the National Science Foundation. We thank Steve Jacobsen for valuable suggestions and two anonymous reviewers for critically reading the manuscript and prompt comments.

REFERENCES

Ammon, C. J., The isolation of receiver effects from teleseismic P waveforms, *Bull. Seis. Soc. Am.*, **81**, 2504-2510, 1991.

Beck, S. L., and G. Zandt, The nature of orogenic crust in the central Andes, *J. Geophys. Res.*, **107**, 2230, doi:10.1029/2000JB000124, 2002.

Beck, S. L., et al., Across the Andes and along the Altiplano: a passive seismic experiment, *IRIS Newsletter*, **13**, 1-3, 1994.

Benz, H., and J. Vidale, Sharpness of upper mantle discontinuities determined from high-frequency reflections, *Nature*, **365**, 147-150, 1993.

Bijwaard, H., W. Spakman, and E. R. Engdahl, Closing the gap between regional and global travel time tomography, *J. Geophys. Res.*, **103**, 30055-30078, 1998.

Bina, C., and G. Helffrich, Phase transition Clapeyron slopes and transition zone seismic discontinuity topography, *J. Geophys. Res.*, **99**, 15853-15860, 1994.

Cahill, T., and B. L. Isacks, Seismicity and shape of the subducted Nazca plate, J. Geophys. Res., **97**, 17503-17529, 1992.

Chen, J., T. Inoue, H. Yurimoto, and D. J. Weidner, Effect of water on olivine-wadsleyite phase boundary in the $(Mg,Fe)_2SiO_4$ system, Geophys. Res. Lett., 29, doi:1810.1029/2001GL014429, 2002.

Collier, J. D., and G. R. Helffrich, The thermal influence of the subducting slab beneath South America from 410 and 660 km discontinuity observations, *Geophys. J. Int.*, **147**, 319-329, 2001.

Dziewonski, A., and D. L. Anderson, Preliminary reference Earth model, *Phys. Earth Planet. Inter.*, **25**, 297-356, 1981.

Engdahl, E. R., R. van der Hilst, and R. Buland, Global teleseismic earthquake relocation with improved travel times and procedures for depth determination, *Bull. Seis. Soc. Am.*, **88**, 722-743, 1998.

Flanagan, M. P., and P. M. Shearer, Global mapping of topography on transition zone velocity discontinuities by stacking SS precursors, *J. Geophys. Res.*, **103**, 2673-2692, 1998.

Gu, Y. J., A. M. Dziewonski, and C. B. Agee, Global de-correlation of the topography of transition zone discontinuities, *Earth Planet. Sci. Lett.*, **157**, 57-67, 1998.

Hasegawa, A. and I. S. Sacks, Subduction of the Nazca plate beneath Peru as determined from seismic observations, J. Geophys. Res., **86**, 4971-4980, 1981.

Helffrich, G., Topography of the transition zone seismic discontinuities, *Reviews of Geophysics*, **38**, 141-158, 2000.

Helffrich, G., and C.R. Bina, Frequency dependence of the visibility and depths of mantle seismic discontinuities, Geophys. Res. Lett., 21, 2613-2616, 1994.

Helffrich, G., and B. Wood, 410-km discontinuity sharpness and the form of the olivine α-β phase diagram: Resolution of apparent seismic contradictions, *Geophys. J. Int.*, **126**, F7-F12, 1996.

Higo, Y., T. Inoue, T. Irifune, and H. Yurimoto, Effect of water on the spinel-postspinel transformation in Mg_2SiO_4, *Geophys. Res. Lett.*, **28**, 3505-3508, 2001.

Hirschmann, M. M., A. C. Withers, and C. Aubaud, Petrologic Structure of a Hydrous 410 km Discontinuity, this volume, 2006.

Karato, S., D. Bercovici, G. Leahy, G. Richard, and Z, Jing, The transition-zone water filter model for global material circulation: Where do we stand?, this volume, 2006.

Katsura, T., S. Yokoshi, M. Song, K. Kawabe, T. Tsujimura, A. Kubo, E. Ito, Y. Tange, N. Tomioka, K. Saito, A. Nozawa, and K. Funakoshi, Thermal expansion of Mg_2SiO_4 ringwoodite at high pressures, *J. Geophys. Res.*, **109**, B12209, doi:10.1029/2004JB003094, 2004.

Katsura, T., and E. Ito, The system Mg_2SiO_4-Fe_2SiO_4 at high pressures and temperatures; precise determination of stabilities of olivine, modified spinel, and spinel, *J. Geophys. Res.*, **94**, 15663-15670, 1989.

Kawakatsu, H., and F. Niu, Seismic evidence for a 920-km discontinuity in the mantle, *Nature*, **371**, 301-305, 1994.

Kennett, B., and E. Engdahl, Traveltimes for global earthquake location and phase identification, *Geophys. J. Int.*, **105**, 429-465, 1991.

Langston, C., Structure under Mount Rainier, Washington, inferred from teleseismic body waves, *J. Geophys. Res.*, **84**, 4749-4762, 1979.

Litasov, K. D., E. Ohtani, and A. Sano, Influence of water on major phase transitions in the earth's mantle, this volume.

Marone, F., S. van der Lee, and D. Giardini, 3D upper mantle S-velocity model for the Eurasia-Africa plate boundary region, Geophys. J. Int., 158, 109-130, 2004.

Pardo-Casas, F., and P. Molnar, Relative motion of the Nazca (Farallon) and South Ameriacan plates since Late Cretaceous time, *Tectonics*, **6**, 233-248, 1987.

Paulssen, H., Evidence for a sharp 670-km discontinuity as inferred from P-to-S converted waves, *J. Geophys. Res.*, **93**, 10489-10500, 1988.

Ringwood, A., Composition and petrology of the Earth's mantle, *McGraw-Hill, New York*, p. 618, 1975.

Shearer, P., Seismic imaging of upper-mantle structure with new evidence for a 520-km discontinuity, *Nature*, **344**, 121-126, 1990.

Smyth, J., and D. Frost, The effect of water on the 410-km discontinuity: An experimental study, *Geophys. Res. Lett.*, **29**, 10.1029/2001GL014418, 2002.

Smyth, J. R. and S. Jacobsen, Nominally anhydrous minerals and earth's deep water cycle, this volume, 2006.

Van der Meijde, M., F. Marone, D. Giardini, and S. van der Lee, Seismic evidence for water deep in Earth's upper mantle, *Science*, **300**, 1556-1558, 2003.

Van der Lee, S., H. Paulssen, and G. Nolet, Variability of P660s phases as a consequence of topography of the 660 km discontinuity, *Phys. Earth Planet. Inter.*, **86**, 147-164, 1994.

Wood, B., The effect of H_20 on the 410-kilometer seismic discontinuity, *Science*, **268**, 74-76, 1995

Wood, B., Postspinel transformations and the width of the 670-km discontinuity: A comment on "Postspinel transformations in the system Mg_2SiO_4-Fe_2SiO_4 and some geophysical implications" by E. Ito and E. Takahashi, *J. Geophys. Res.*, **95**, 12681-12688, 1990.

Yamazaki, A., and K. Hirahara, The thickness of upper mantle discontinuities, as inferred from short-period J-array data, *Geophys. Res. Lett.*, **21**, 1811-1814, 1994.

Jochen Braunmiller, Institute of Gephysics, ETH Zurich, 8093 Zurich, Switzerland, jochen@sed.ethz.ch